VALIDATION OF BUBBLE SIZE MEASUREMENTS WITH WIRE-MESH SENSORS BY HIGH-SPEED VIDEO OBSERVATION

D. Scholz, C. Zippe

Forschungszentrum Rossendorf e.V., P.O.Box 510119, D-01314 Dresden, Germany
e-mail: prasser@fz-rossendorf.de

1 Introduction

In the following presentation, I want to introduce the results, which were obtained by a comparison between values of bubble sizes of the wire-mesh sensor and values obtained by video-observation. The task was an investigation of the accuracy of bubble sizes measured by the wire-mesh sensor. A second task was the determination of the lower limit of bubble sizes, which is resolved by the sensor. For bubbles with a diameter smaller than the distance between the wires of the mesh, this was an important question.

The production of bubbles with a definite volume respectively size is hardly possible. Therefore a direct comparison with the measurement data of sensor is impossible. We decided to use another method for a comparison. It should be based on another measuring technique. We had observed the movement of bubbles with a high-speed video device. The measurement of the sensor and the observation were started simultaneously. So, it was possible to compare both results. An important condition was the use of a transparent test channel.

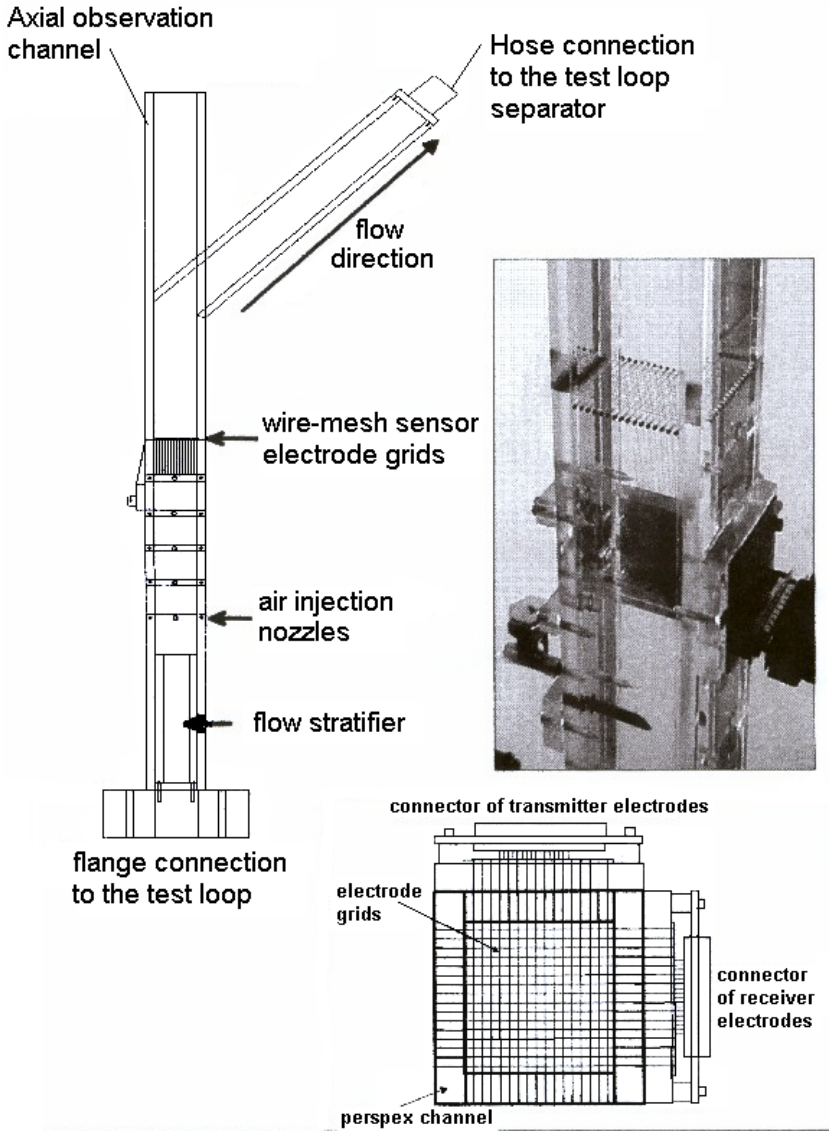

Fig. 1 Perspex channel with wire-mesh sensor

2 Organic glass channel

The electrodes of a wire-mesh sensor were built into a transparent test channel made of organic glass (Fig. 1). This channel has a square cross section with an inner width of 50 mm. The sensor consists of 16 transmitter and 16 receiver electrodes each. The pitch between the individual electrodes is 3.125 mm. The gap between the electrode planes is 1.5 mm. One end of each electrode is going through the channel wall and connected with a plug connector outside.

The wire-mesh sensor was operated with a measuring frequency of 1000 Hz (frames per second). All experiments were performed under identical environmental conditions. For this purpose the test channel was mounted on the two-phase flow test-loop (MTLoop) of the institute. For the experiments, water flows with liquid velocities between 0.05 and 0.8 m/s were produced in the loop. Air bubbles were generated using different injection nozzles. For the investigation it was very important to generate bubbles rising separately in the liquid flow. Three different nozzles were installed one after the other in an orifice below the sensor. The local pressurised air net was used for the air supply. The flow was adjusted to a gas velocity of 0.005 m/s.

3 Test set-up

The test set-up consisted of the wire-mesh sensor and a high-speed video device. With this set up the transition of bubbles through the sensor electrodes was observed. The digital video recorder worked with a speed of 1000 frames per second. This is the same frequency like the measuring frequency of the sensor. The important

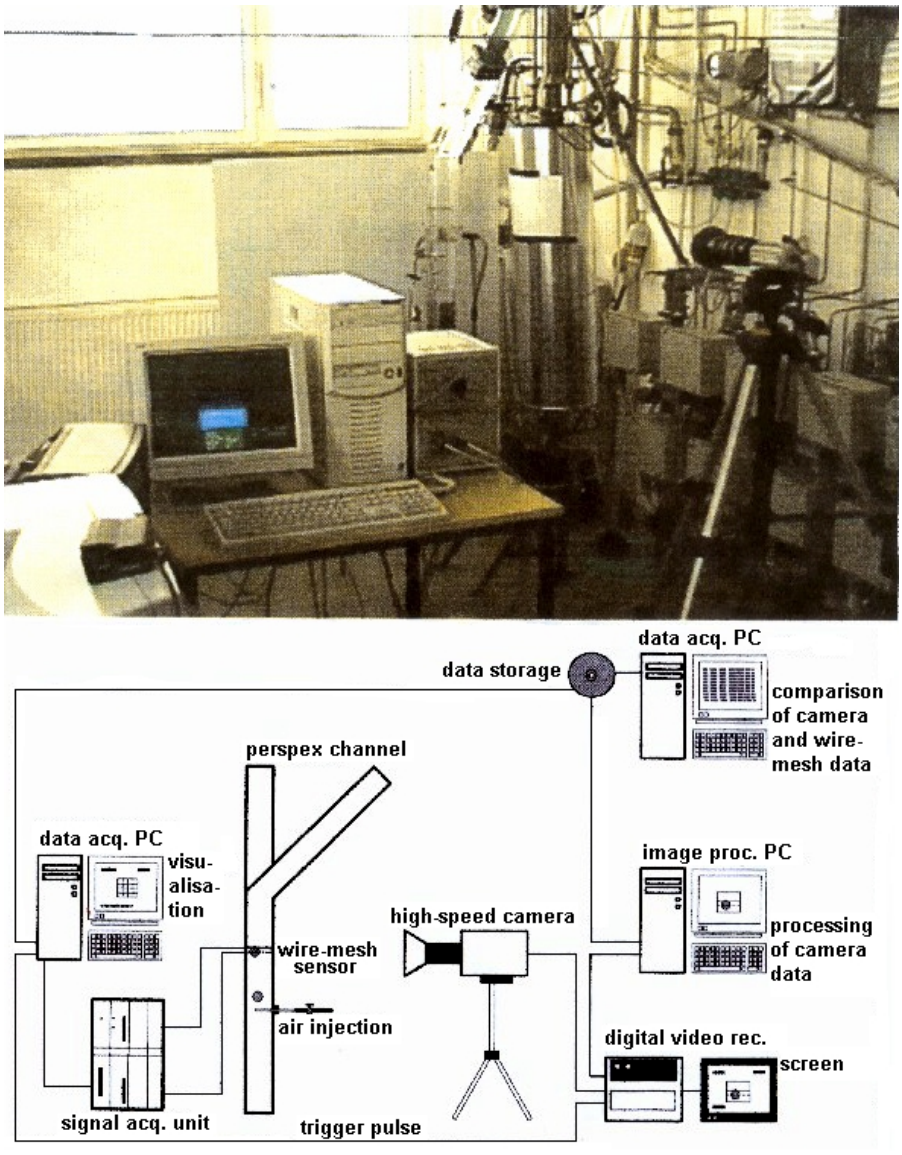

Fig. 2 View of the test channel at the two-phase flow test loop

components are shown in Fig. 2. Apart from sensor and camera, computers for the analysis belong to the set-up.

Wire-mesh sensor and the video device were started simultaneous. That was realised by a trigger signal, which was generated when the start button on the data acquisition computer of the wire-mesh sensor was pressed. The video device was started by this trigger signal. All data of measurement and observation were analysed by a external computer.

Very important is the accurate alignment of the high-speed camera. In the captured frame, just the sensor and his immediate environment should be visible. The width of a frame should be equal to the inner width of the channel. The camera was adjusted in a way that the orientation of the pixel lines was accurately in the horizontal direction of the measuring plane. This were important conditions for a optimum analysis. A video sequence consists altogether of 8738 separate frames of 256 x 240 pixels.

4 Evaluation of camera frames

The main problem was to calculate the volume size respectively the bubble size from the two dimensional view obtained by the camera. For this we used a procedure, which is introduced in Fig 3.

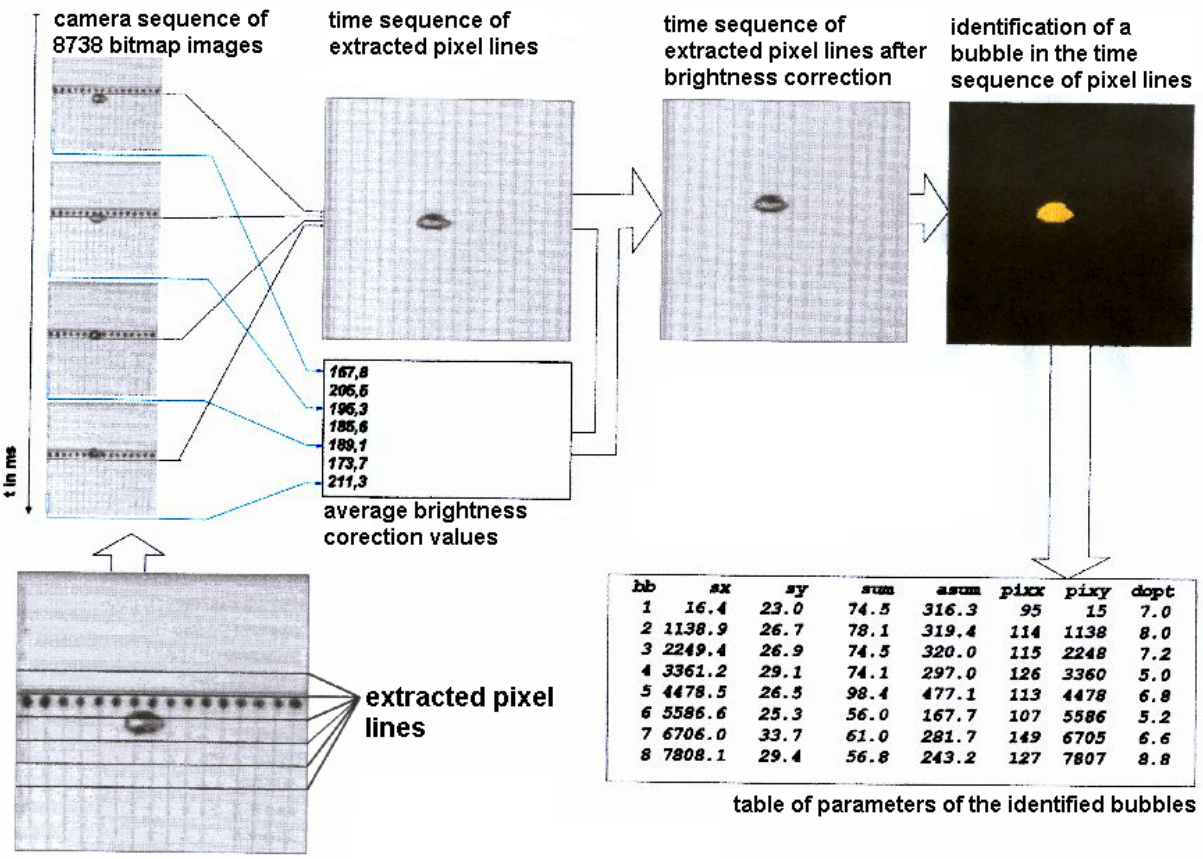

Fig. 3 Extraction of Eulerian sectional side views from camera sequences and optical bubble recognising method

The frames of a video sequence were saved as bitmap files. Every file consists of 256 x 240 picture elements (pixels). A frame corresponds to a time range of 1 ms, which is given by the recording speed of 1000 frames per second. Lines of pixels are taken out of every frame of a sequence from an identical selected axial position. All these lines are merged to create a new bitmap file, where the lines are stacked on top of each other, forming a new image of as many lines as individual frames are in the time sequence. The algorithm starts with the pixel line from the first frame on top of the new image, the successive lines are put in the order from the top to the bottom. This new file has altogether 8738 lines now. It represent a Eulerian pseudo-side view of the flow, where the vertical axis is a time axis. This kind of operation was performed for six different axial positions in the original camera frames: the line exactly located in the gap between the electrode grids, four lines below the measuring plane at different distances and one line above the measuring plane.

The projections extracted in this way were used to determine bubble sizes. For the comparison with the bubble size measured by the wire-mesh sensor the first line below (upstream) the sensors was used. In this place, the bubbles still have their undisturbed shape. The image is processed to correct the 100 Hz oscillations of the illuminating lamps. In the next step, a threshold was applied to binarize the bubble shape. By the help of a recursive fill algorithm, inner pixels, which were not recognised as air due to optical reflections were assigned to the gas phase domain. In the last step, the bubble volume was assessed assuming a rotational symmetry (Fig. 4). The diameter was calculated by taking the cubic root of the volume. These data about size and the position of the bubbles in the flow are stored in a table. The values in the table will be used for the comparison with the values from wire-mesh sensor.

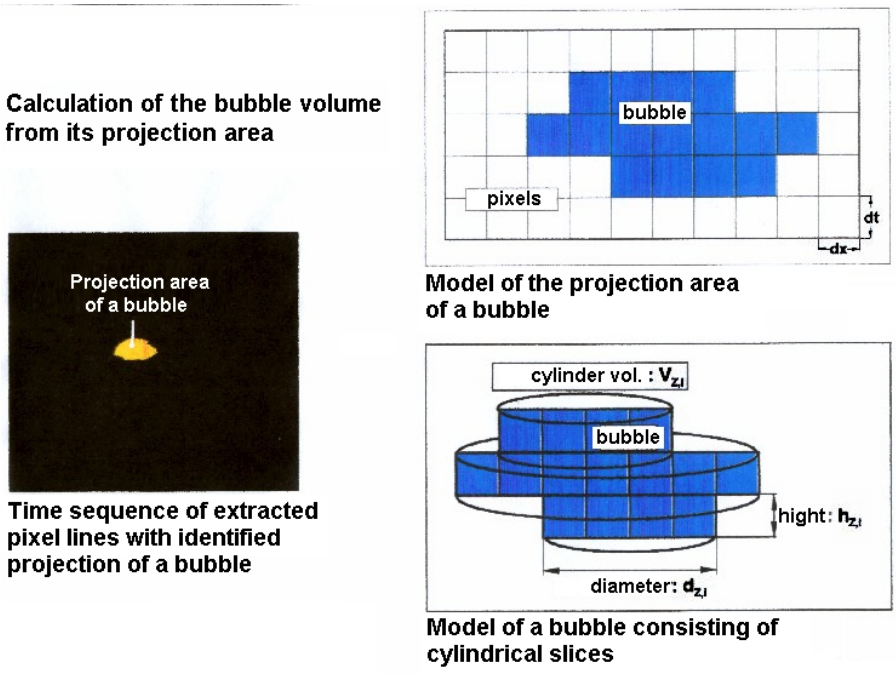

Fig. 4 Optical bubble size estimation

The presence of rotational symmetry was assumed for each horizontal layer of the bubble of the thickness of one pixel (Fig. 4). The visible surface of bubble in the projection consists of a certain number of lines with a certain number of pixels identified to belong to the bubble. Each horizontal line of pixels of the bubble image was treated as the side view of a cylinder. The cylinder diameter can be calculated from the number of pixels and the cylinder height (in units of time) is known, because a line correspond with a time range of one millisecond. So, the cyl-

inder volume will be calculated by adding the results for each line occupied by the bubble.

The visible surface in the projection does not represent the real appearance of the bubble, because the vertical axis is a time axis. The volume is therefore related to the bubble velocity and measured in units of $m^2 \cdot s$, the diameter in units of $(m^2 \cdot s)^{1/3}$. This is not a disadvantage, since the wire-mesh sensor can deliver real volumes only if the bubble velocity is known. Therefore it is better to compare related volumens respectively related diameters. In this case, the additional measuring error caused by the uncertainty of any velocity information is excluded.

Table of bubble parameters obtaind by the wire-mesh sensor

im	jm	km	mi	mj	mk	mr	max	v	r	n	deps
2266.8	28.5	28.3	10.1	4.6	3.3	8.2	81	370	4.45	481	0.0016916
4495.7	29.3	19.5	8.3	3.8	3.3	6.9	75	293	4.12	362	0.0013434
6723.0	22.4	24.9	7.7	4.6	3.5	6.8	74	306	4.18	379	0.0014010
31.2	32.3	25.5	8.7	3.3	4.2	7.2	70	288	4.10	379	0.0013192
3378.5	27.6	24.5	6.6	3.7	3.6	6.0	68	255	3.64	270	0.0009222
5604.7	32.7	24.8	9.6	3.3	4.5	7.8	68	351	4.38	432	0.0016062
1154.6	29.6	26.0	8.8	3.5	3.6	7.2	65	283	4.07	357	0.0012937
7825.0	26.1	20.3	7.7	4.1	3.7	6.7	65	324	4.26	377	0.0014851

Table of bubble parameters obtained from the camera sequences

bb	sx	sy	sum	asum	pixx	pixy	dopt
1	16.4	23.0	74.5	316.3	95	15	7.0
2	1138.9	26.7	78.1	319.4	114	1138	8.0
3	2249.4	26.9	74.5	320.0	115	2248	7.2
4	3361.2	29.1	74.1	297.0	126	3360	5.0
5	4478.5	26.5	98.4	477.1	113	4478	6.8
6	5586.6	25.3	56.0	167.7	107	5586	5.2
7	6706.0	33.7	61.0	281.7	149	6705	6.6
8	7808.1	29.4	56.8	243.2	127	7807	8.8

Table of parameters of corresponding bubbles from both wire-mesh sensor and camera

ds	max	sx	sz	dr	d1	d2	d3	d4	d5
8.9	81	121	2266	8.3	10.2	8.5	8.1	8.2	8.3
8.2	75	115	4494	9.0	9.5	9.7	9.7	9.5	9.9
8.4	74	149	6720	7.8	9.8	8.1	7.7	7.8	8.1
8.2	70	99	31	8.2	8.0	8.5	8.1	9.8	8.9
7.9	68	123	3376	7.6	9.3	8.3	8.2	8.0	8.1
8.8	68	98	5603	8.3	8.1	6.8	8.3	8.1	7.9
8.1	65	112	1154	8.4	8.8	8.5	9.8	9.8	8.9
8.5	65	131	7823	7.1	10.5	7.7	7.4	7.9	9.2

Fig. 5 Comparison between wire-mesh and camera data

5 Comparison of data

The bubble sizes measurement with the wire-mesh sensor was carried out according to the method described in [1]. The sizes and the positions of the bubbles, which were determined by wire-mesh sensor, were saved in a similar table like the data from video observations. Related volumes and respectively related diameters were calculated to make it unnecessary to measure the bubble velocity. The data from the table of camera data and the table of the wire-mesh sensor data were merged by selecting the lines that belong to identical bubbles and putting them into a new table in one line (Fig. 5). This table contains the optically obtained related diameter and the related diameter measured by the wire-mesh sensor of one and the same bubble in one line. These points can be plotted in a co-ordinate system for the two mentioned values (Fig. 6). The different experimental conditions for the points shown in Fig. 6 are summarised in Fig. 7. In this table all fifteen measurements are listed. The experiments were carried out with the three different air nozzles and different liquid velocities ranging from 0.05 to 0.8 m/s. The presence of a code number indicated the availability of the given combination of velocity and injection capillary. The code itself was used as file name and contains the date of the measurement and a successive number.

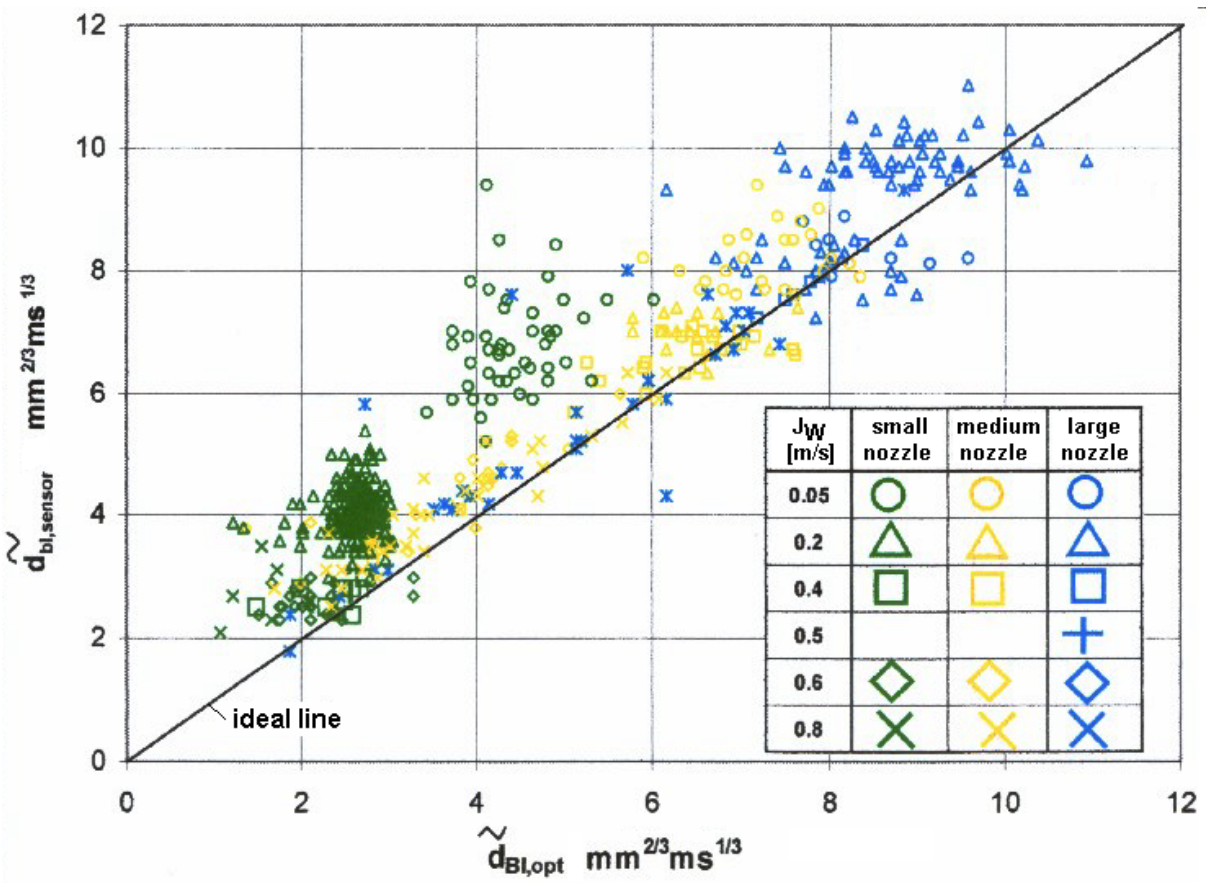

Fig. 6 Comparison of related bubble diameters

As shown in Fig. 6, the agreement between the two methods is satisfying. There is a tendency to overestimate the bubble size by the wire-mesh sensor for low diameters and low liquid velocities. This may be caused by the finite axial extension of the measuring plane of the wire-mesh sensor, which is 1.5 mm high. This leads to the

effect, that each bubble is virtually prolonged in axial direction by a contribution of this order of magnitude. The relative effect of this systematic error is increasing with decreasing bubble size, so that the agreement is better for bigger bubbles.

Flow velocity of water [m/s]	small nozzle	medium nozzle	large nozzle
0,05	19060004	19060001	16060001
0,11			16050001
0,20	19060005	19060002	15060001/16060003
0,33			17050001
0,40	22060003	19060003	16060002
0,50			22060002
0,60	20060001	20060003	22060001
0,67			17050002
0,80	20060002	20060004	

code numbers indicate realised measurements (file names)

Flow velocity of water [m/s]	small nozzle
0,05	13070001
0,40	13070002
0,60	13070003

Measurements carried out with enlarged camera view field (macro zoom)

Fig. 7 Summary of conducted experiments at the transparent test channel

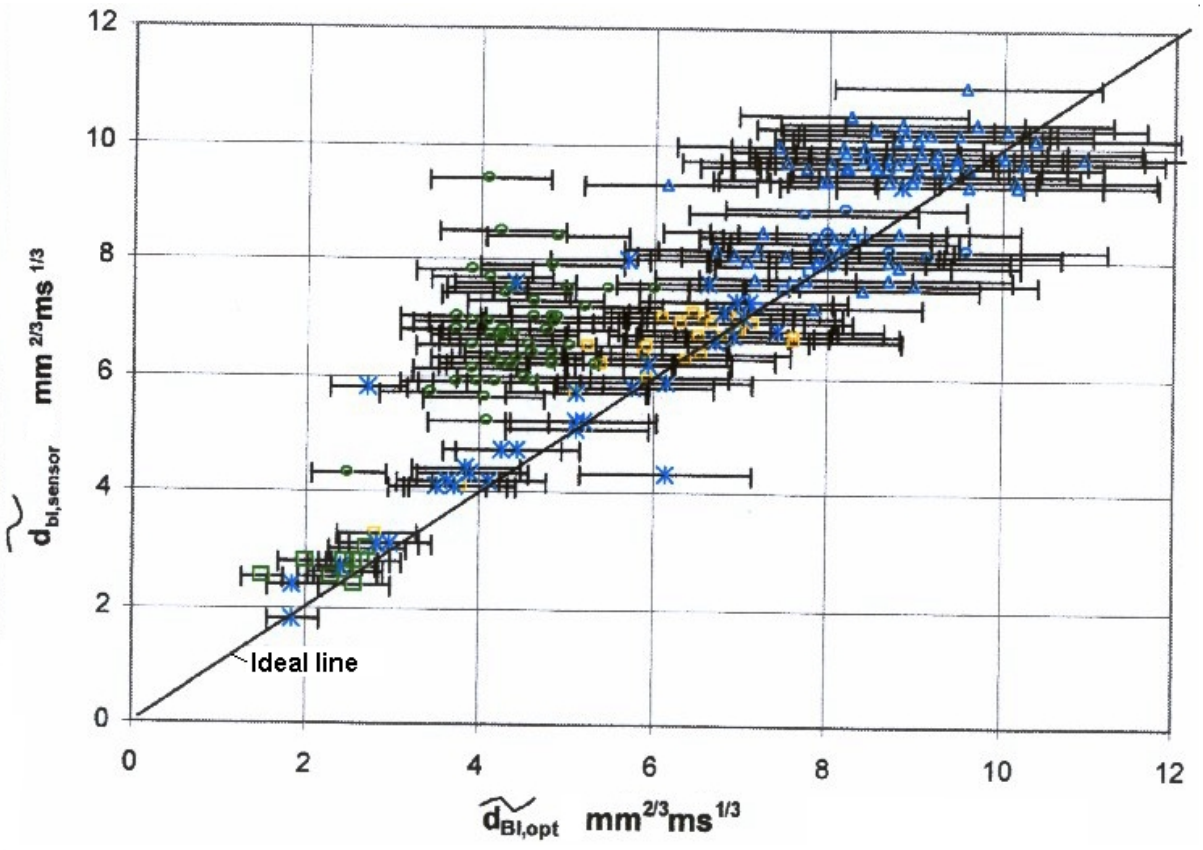

Fig. 8 Assessment of the measuring error of the optical bubble size determination

6 Estimated error

An important question is the assessment of the measuring accuracy of the optical bubble size measurement. A investigation had shown that the influence of this error was high. Therefore the error sources were searched. We found four mainly sources: The largest error contribution is caused by the fluctuation of bubble shape. In reality, the bubbles do not have a rotational symmetry. Their horizontal extension can change depending on the view direction. Other errors arise due to the parallaxes and due to the discretization of the camera frames. The total relative error of the related bubble diameter obtained by the optical method was found to be about 19%. Corresponding error bars are introduced in Fig. 8. Together with the error bars most of the measuring points include the ideal line.

7 Resolving capability of the wire-mesh sensor

A other task was the determination of the lower limit of bubble sizes, which is just resolved by the wire-mesh sensor. It was found, that the relative position of the centre of a bubble in the grid of crossing sensor wires has an influence on the appearance of the bubble in the sensor signal. In general, the relative position of the bubble centre related to the cross points of the wires is arbitrarily changing. In a turbulent two-phase flow an equal statistical distribution

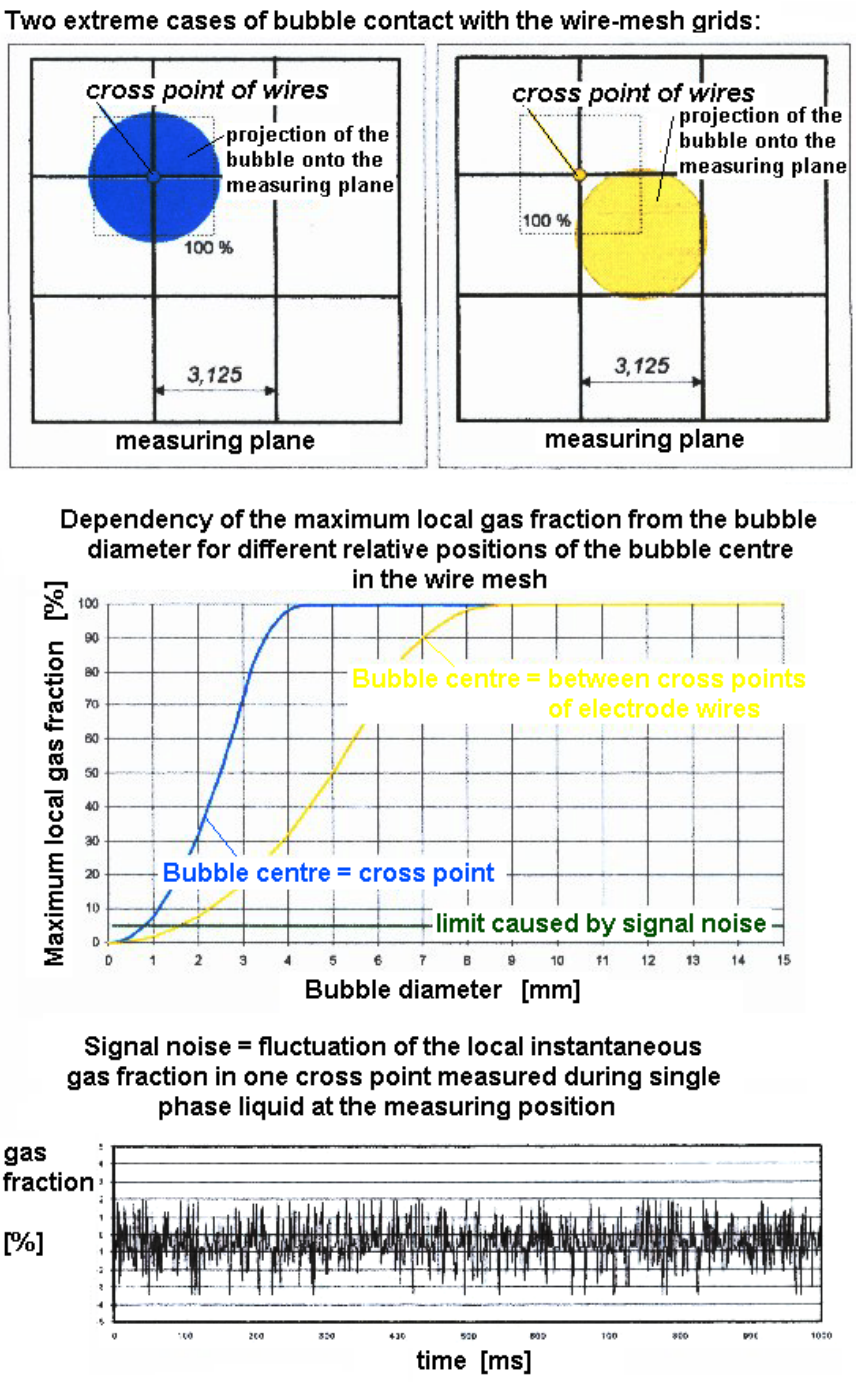

Fig. 9 Model to assess the bubble size resolution limits of the wire-mesh sensor

of the location of the bubble centre can be assumed. If the bubble passes the sensor plane in a way that the centre of the bubble is corresponding to the centre of one mesh (Fig. 9, right side), then the maximum observed local instantaneous gas fraction during the bubble passage is on minimum for a given bubble size, when the centre is located at the cross point of two wires (Fig. 9, left side), then the maximum observed local instantaneous gas fraction is on maximum.

From simple geometrical considerations it can be concluded, that the diameter of the bubble must be greater than the double length of the diagonal of one electrode mesh to ensure that the mesh can be covered by the bubble completely. Bubbles greater than this diameter should always show maximum local instantaneous gas fractions of up to 100 %. If the bubble diameter is equal to one length of the diagonal, it can still produce instantaneous local gas fraction values, but only if it passes through the measuring plane exactly in a way, that the bubble centre goes through the cross point of two wires. This is reflected by the yellow and the blue curves in the lower part of Fig. 9, where theoretical maximum values are presented. They were calculated under the assumption that the maximum of the local instantaneous gas fraction is approximately equal to the shading of the most affected square control volume by the bubble, i.e. the visible surface of the bubble and the sensitive volume by a view from above were put in proportions. The result values were plotted in a diagram, in which the maximum local instantaneous gas fraction is plotted against the real bubble diameter.

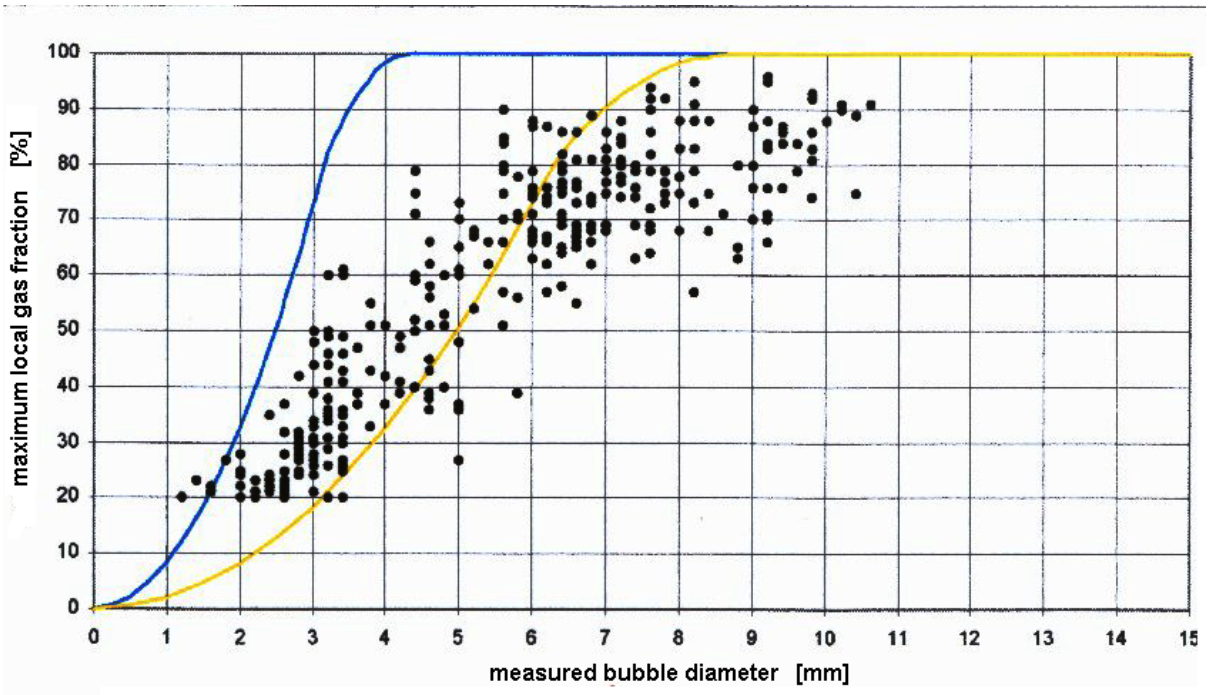

Fig. 10 Measured maximal gas fractions inside of bubbles depending on their diameter

For all fifteen experiments listed in Fig. 7, points characterising the maximum of the local instantaneous gas fraction observed within a bubble and the corresponding measured bubble diameter were put into the diagram developed in Fig. 9 for all registered bubbles. The bubble diameters were determined likewise from the video frames. The result is shown in Fig. 10. We can see, that small bubbles with a di-

ameter smaller than the range of electrodes, are situated between the blue and yellow limits. This means that the simple geometric assumptions leading to the yellow and blue limits are confirmed. If we now consider the noise level of the raw signal, which was found to be around 7 % in the given experimental set-up, then the diameter of the smallest bubble which can still be detected with a probability of 100 % can be found at the point, where the maximum gas fraction for the yellow curve becomes less than the noise level, which is the case for bubbles less than approximately 1.5 mm. Bubbles with diameters less than this value can still be detected if they are greater than about 1 mm, but the probability to detect them is no more 100 %. Smaller bubbles cannot be resolved at all. To increase resolution, the noise level must be decreased, which can be managed to a certain extend by better electrical screening.

Further we can see, that gas fractions of 100 % were not reached in the experiments. This is caused by so-called water bridges, which developed due to the fragmentation and deformation of the bubbles at the sensor wires.

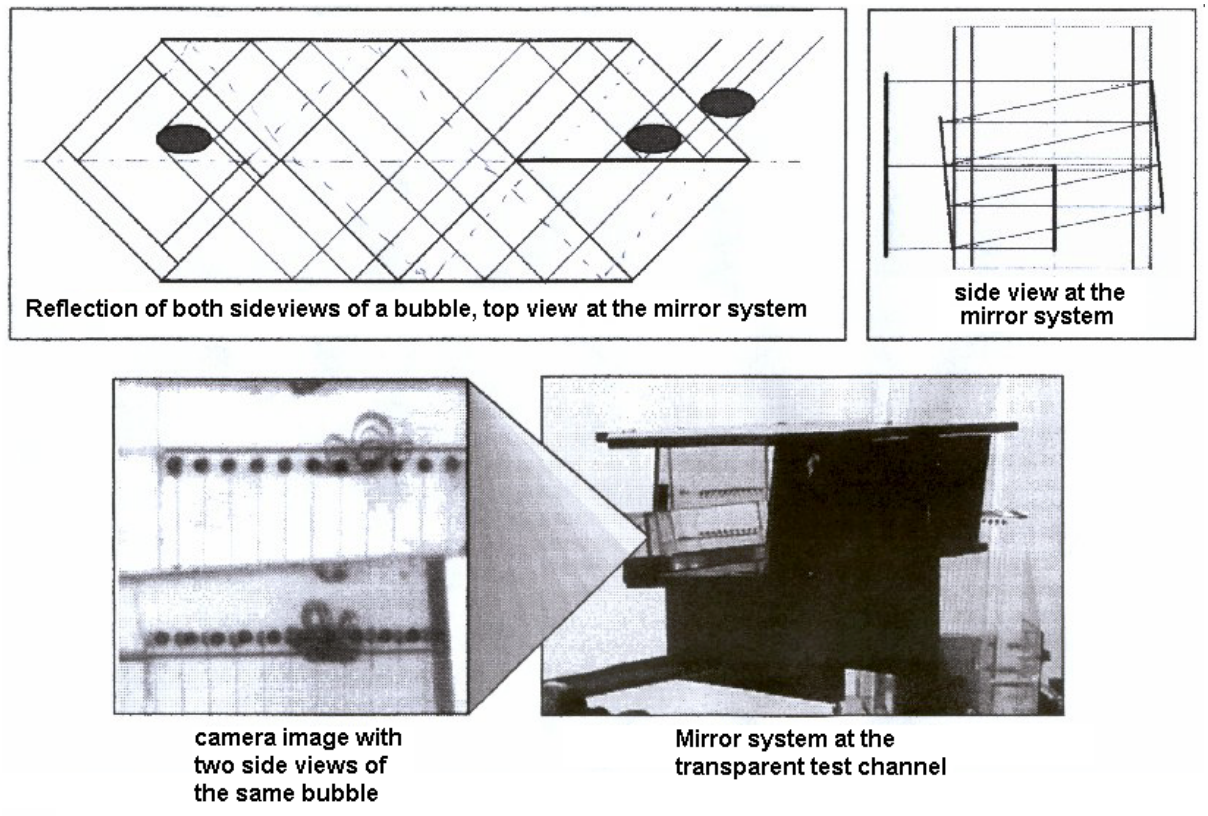

Fig. 11 Mirror system for stereoscopic video observations of bubbles in the wire-mesh sensor

8 Mirror optic for stereoscopic observations

The measuring error of the optical bubble size measurement can be decreased by observing the bubble from two perpendicular directions. For this purpose, a stereoscopic visualisation system was developed (Fig. 11). It consists of a mirror assembly that produces a compound image consisting of an upper part showing the test channel from one direction and a lower part, showing it from the other direction. In this

way, the horizontal resolution of the digital video system can be optimally utilised. Preliminary tests have shown, that the mirror optic is functioning, but has still some deficiencies. In the next time it will be redesigned and afterwards used for new experiments.

9 Conclusions

The investigations have shown that the determination of bubble sizes with the wire-mesh sensor is possible. It is also possible to determine the bubble size of bubbles with diameters smaller than the pitch of the sensor electrodes. The smallest detectable bubble diameter depends on the signal noise level. In the experiments carried out the lowest resolved bubble diameter was around 1.6 mm.

The error of image analysis amounts to approximately 19 %. Therefore, this error has a big influence to the result of the comparison. The goal was set to improve the image processing by using a stereoscopic visualisation of flow.

10 Literature

[1] H.-M.Prasser: Messung von Blasengrössenverteilungen mit Gittersensoren, Workshop „Messtechnik für stationäre und transiente Mehrphasenströmungen“, 24.-25.September 1998 in Rossendorf, FZR-241, November 1998, S. 157-164.

[2] H.-M. Prasser, A.Böttger, J.Zschau: A new electrode-mesh tomograph for gas-liquid flows, Flow Measurement and Instrumentation 9, 1998, S.111-119.

[3] H.-M.Prasser: Leitfähigkeitssensoren für die Bestimmung von Parametern in einer Zweiphasenströmung, Workshop „Messtechnik für stationäre und transiente Mehrphasenströmungen“, 6.-7. November 1997 in Rossendorf, FZR-204, Dezember 1997, S. 64-71.

[4] D. Scholz: Bewertung der Genauigkeit eines Gittersensors zur Visualisierung einer Zweiphasenströmung durch Vergleich mit optischen Hochgeschwindigkeitsaufnahmen, Diplomarbeit, Rossendorf, September 2000.